CFD Prediction of Wind Turbine Blade Compressible Aerodynamics

A. Mezzacapo, M. C. Vitulano, A. D. Tomasso, and G. De Stefano(✉)

Engineering Department, University of Campania Luigi Vanvitelli, Aversa 81031, Italy
giuliano.destefano@unicampania.it

Abstract. Computational fluid dynamics (CFD) analysis is carried out to evaluate the compressible aerodynamics of a large horizontal axis wind turbine blade. The mean turbulent flow around the rotating blade is simulated by adopting the unsteady Reynolds-averaged Navier-Stokes modelling approach, where the governing equations are solved by means of a finite volume-based numerical method, supplied with a two-equation eddy-viscosity turbulence model. The present CFD model using an open-source code for computational wind engineering applications was verified to have significant practical potential by making a comparison with a reference steady solution.

Keywords: Computational Wind Engineering · Compressible Flow · Turbine Blade Aerodynamics · Open Source Software

1 Introduction

To meet the global energy demands, the size of wind turbines (WT) is getting larger and larger, in order to maximize power generation. This holds, in particular, for offshore systems that can be installed in deep water locations, where very large rotors are able to generate higher power due to high wind speeds. Therefore, the trend of adopting very large rotor diameters and high tip-speeds has brought about a renovated interest in the aerodynamic design of wind turbine blades, where significant compressibility effects have to be taken into account [1,2]. In fact, the aerodynamic design of large wind turbines represents a very challenging task, calling for deep innovations in the scaled-up design methodology [3].

Computational fluid dynamics (CFD) analysis is heavily used as a base method for analyzing WT designs [4], with the Reynolds-averaged Navier-Stokes (RANS) modeling approach being usually followed [5]. In the computational wind engineering (CWE) domain, however, past compressible studies were mostly conducted for airfoil flows, e.g. [6]. Concerning previous three-dimensional simulations, as either the WT sizes were not large enough, or the tip speeds were not high enough, much more research is needed for better investigating the aerodynamic properties of these novel systems, including compressibility effects.

© The Author(s), under exclusive license to Springer Nature Switzerland AG 2023
O. Gervasi et al. (Eds.): ICCSA 2023, LNCS 13956, pp. 113–125, 2023.
https://doi.org/10.1007/978-3-031-36805-9_8

Table 1. IEA-15-240-RWT: relevant parameters.

Parameter	Value
Power	15 MW
Rotor diameter	240 m
Rotor speed	7.56 rpm
Maximum tip speed	95 m/s
Hub height	150 m
Wind speed	10.6 m/s

Table 2. IEA-15-240-RWT: blade geometric parameters.

Parameter	Value
Blade length	117 m
Root diameter	5.20 m
Root cylinder length	2.34 m
Max chord	5.77 m
Max chord spanwise position	27.2 m
Tip prebend	4.0 m

This study deals with the three-dimensional model of a horizontal axis wind turbine (HAWT) that represents the most common design for modern large machines. The blade under investigation belongs to the IEA Wind 15 MW offshore reference wind turbine (RWT) that was recently released [7]. Specifically, the model data for the present work were originally developed within the International Energy Agency (IEA) Wind Task 37 on wind energy systems engineering [8]. Some key parameters of this three-bladed machine, which is referred to as IEA-15-240-RWT, are given in Table 1. It represents a standard design model that can be used for concept studies, like the present one, as the wind energy industry progresses toward larger systems. Given the blade length and the maximum tip speed, the compressible regime is indeed approached.

The main goal of the present work is the computational evaluation of the compressible aerodynamics for the single blade of the above RWT, using open-source CFD software that is available to the industrial researchers. Differently from similar works, where compressibility corrections were employed, the compressibility effects are directly simulated. Specifically, the mean turbulent flow past the rotating blade is predicted by using the open-source code OpenFOAM, employing the finite volume (FV) discretization approach, supplied with an unsteady RANS turbulence modeling procedure.

The rest of this paper is organized as follows. In Sect. 2, the overall CFD model is introduced, including details about the blade geometry, the computational domain, the turbulence closure, and the numerical method. The results of the simulations are made known and discussed in Sect. 3. Finally, some concluding remarks are drawn in Sect. 4.

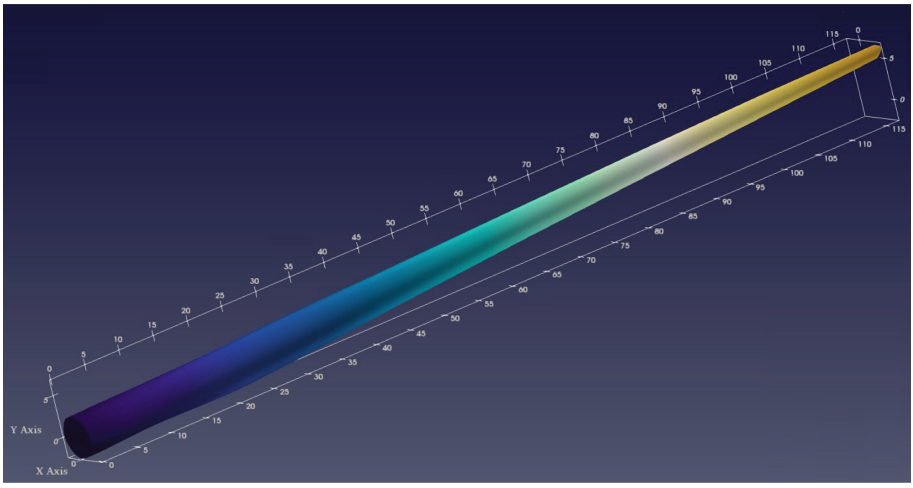

Fig. 1. Computational geometry of the RWT blade.

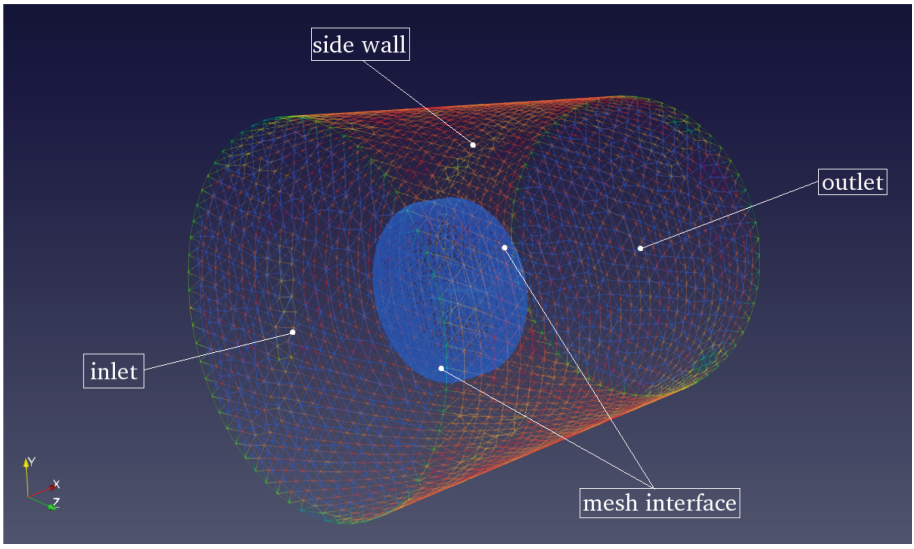

Fig. 2. Sketch of the computational domain: rotating mesh, represented by the inner cylinder including the blade, along with the outer stationary mesh.

2 CFD Model

2.1 Case Study

The computer-aided design (CAD) geometry of the IEA-15-240-RWT blade model was taken from [8], where it is publicly available. Some relevant geometric parameters of this model are summarized in Table 2. The DTU FFA-W3

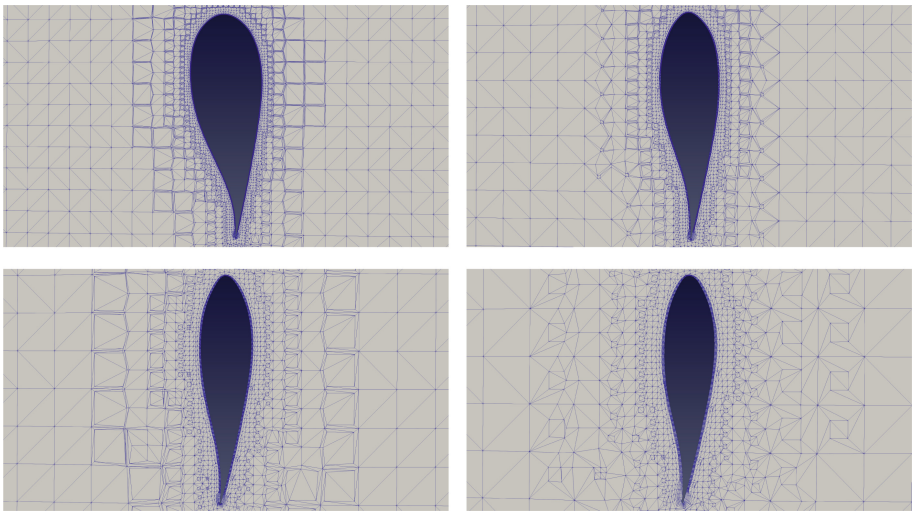

Fig. 3. Cross-plane views of the computational mesh around the blade, corresponding to sections at 40% (top left), 60% (top right), 80% (bottom left), and 90% (bottom right) of its length.

series of airfoils was used in the blade design. These well-documented airfoils were also used in the IEA Wind/DTU 10 MW offshore RWT [4], for instance. The blade rotates around the horizontal X axis with constant angular velocity, say Ω. Figure 1 shows the CAD geometry, with the rotating blade occupying the instantaneous position along the Z axis direction.

2.2 Computational Domain

The computational domain was constructed by employing two nested coaxial cylinders, with the cylinder axis being horizontal. The inner cylinder, which has a length of 60 m and a radius of 150 m, rotates together with the blade, while the outer one, which has a length of 1050 m and a radius of 350 m, remains stationary. The inner part of the computational domain is created around the blade model depicted in Fig. 1. Practically, some of the air that flows in the inlet of the outer domain passes through the inner rotating domain.

Two different meshes are constructed, independently, for the two above subdomains. Since the inner cylinder mesh rotates with respect to the outer cylinder one, the interface between the two sliding meshes is handled by a special boundary condition referred to as arbitrary mesh interface (AMI). The present work follows a similar approach adopted in past studies for the CFD simulation of smaller turbines [9].

The computational domain is sketched in Fig. 2, which shows the rotating mesh, represented by the inner cylinder including the blade, along with the outer stationary mesh. Note that these ones are not the true meshes, but coarser ones used for illustration only. In fact, the results presented in the following were obtained using an overall mesh consisting of about 5 million FV cells. The mesh was suitably refined in the space region close to the blade surface, including the near wake. For illustration, in Fig. 3, the cross-plane views of the FV mesh are shown at four different stations along the blade, namely at 40%, 60%, 80%, and 90% of its length.

Table 3. Types of boundary conditions for mean flow variables.

Boundary	**Velocity**	**Pressure**	**Temperature**
Inlet	fixedValue	zeroGradient	fixedValue
Outlet	inletOutlet	inletOutlet	inletOutlet
Side wall	slip	zeroGradient	zeroGradient
Blade	movingWallVelocity	zeroGradient	zeroGradient
AMIs	cyclicAMI	cyclicAMI	cyclicAMI

Table 4. Types of boundary conditions for turbulence variables.

Boundary	**Kinetic-energy** k	**Specific dissipation** ω
Inlet	fixedValue	fixedValue
Outlet	inletOutlet	inletOutlet
Side wall	fixedValue	fixedValue
Blade	kqRWallFunction	omegaWallFunction
AMIs	cyclicAMI	cyclicAMI

2.3 Unsteady RANS Model

The mean compressible flow around the blade was described by the unsteady RANS governing equations. These equations, which are not reported here for brevity, can be found in [5], for instance. The governing equations were supplied with suitable boundary conditions for the mean velocity, pressure, and temperature, as summarized in Table 3. The ambient temperature and pressure levels were set to standard values that are $T_\infty = 293\ K$ and $p_\infty = 101325\ Pa$, respectively. The freestream conditions corresponded to a uniform horizontal wind with constant velocity that was $U_\infty = 10.59\ m/s$. The latter was imposed at the inlet, along with the zero gradient boundary condition for the mean pressure field. Note that the blade surface was assumed as an adiabatic rotating wall with the constant angular velocity $\Omega = 0.79\ rad/s$. These operating conditions correspond to the theoretical parameters of the IEA-15-240-RWT model that are

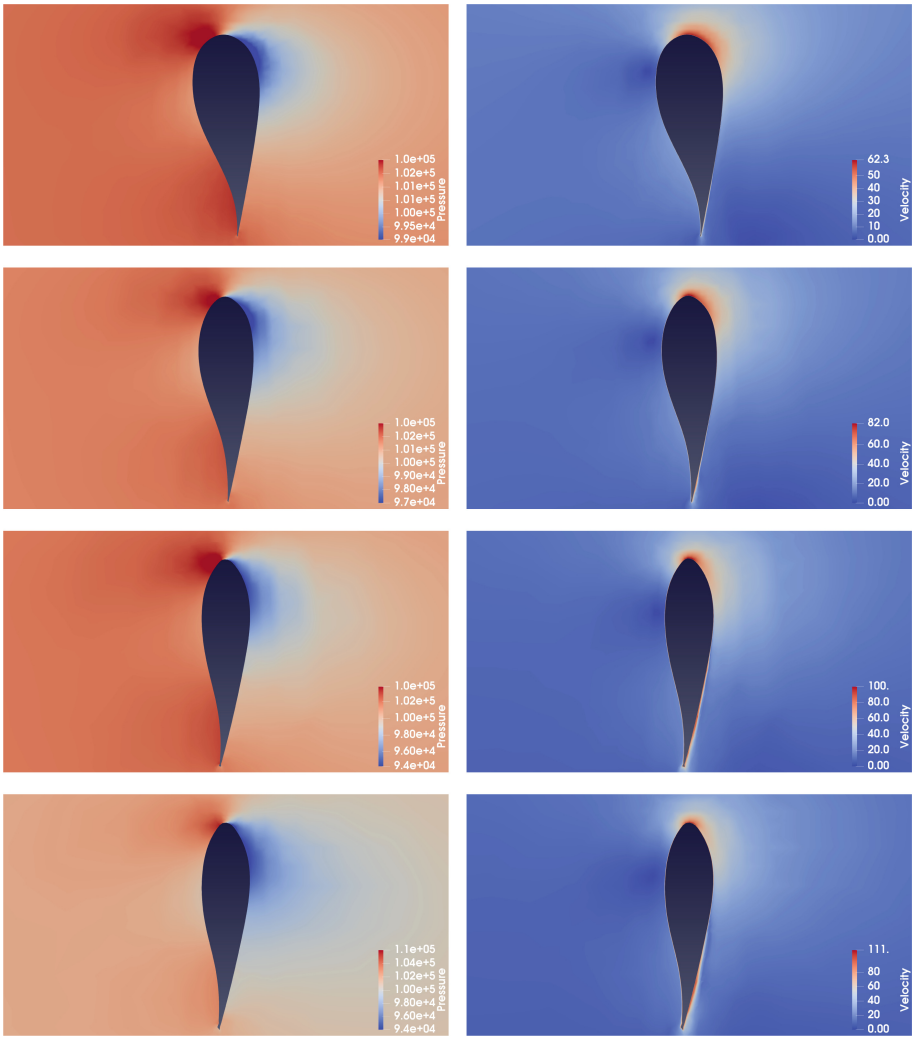

Fig. 4. Contour maps of pressure (left) and velocity modulus (right) around the blade, for four different cross-sections, corresponding to 40% , 60%, 80%, and 90% of its length (from top to bottom).

given in Table 1. Also, slip wall boundary conditions were used at the side wall of the virtual wind tunnel, while the no-slip boundary condition was imposed on the blade surface.

As is usual for industrial aerodynamics applications, eddy viscosity-based diffusion was introduced into the mean flow equations to mimic the effects of

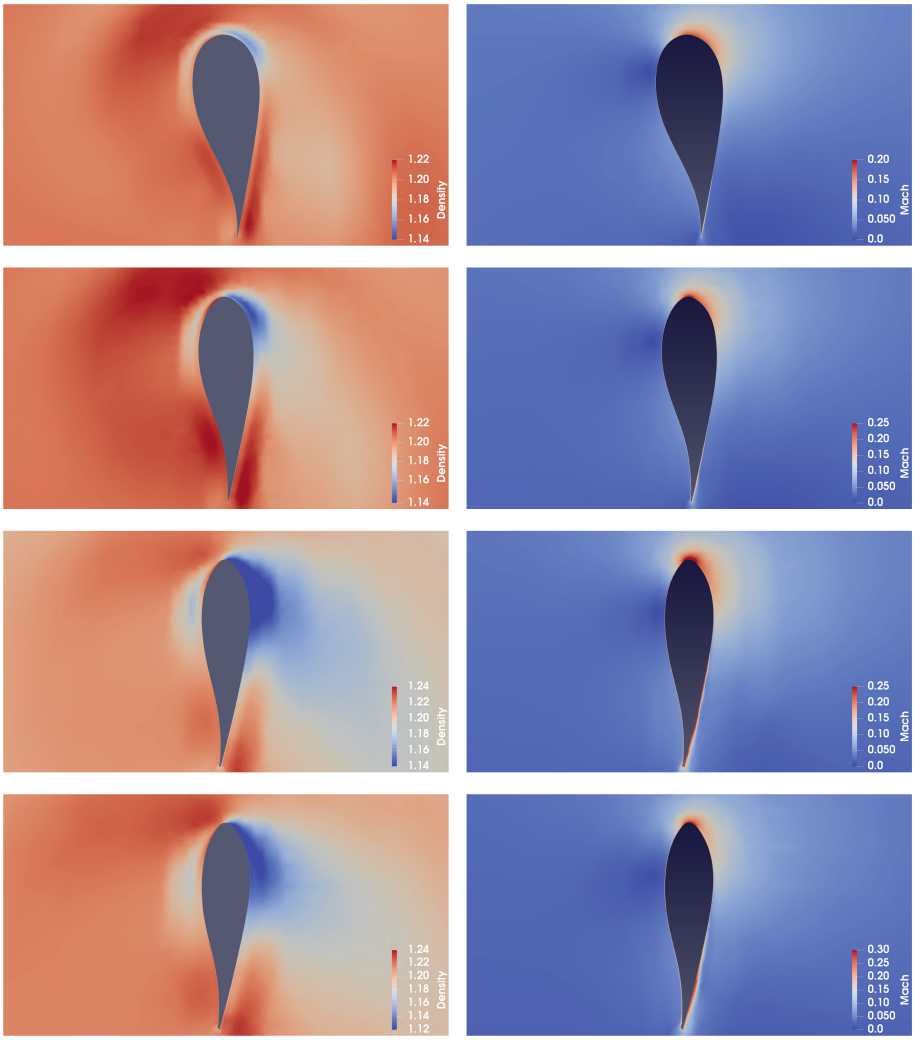

Fig. 5. Contour maps of density (left) and flow Mach number (right) around the blade, for four different cross-sections, corresponding to 40% , 60%, 80%, and 90% of its length (from top to bottom).

turbulence [10,11]. In this work, the k–ω SST two-equation turbulence model [12] was employed, where two additional evolution equations for the turbulent kinetic energy k and the specific turbulent dissipation rate ω are solved to determine the instantaneous pointwise eddy-viscosity parameter. Note that this model is commonly used for computational wind engineering applications [6]. The boundary



Fig. 6. Surface distribution of relative pressure Δp (Pa) on pressure (top) and suction (bottom) sides of the blade.

conditions that were imposed for these two additional variables are summarized in Table 4. The fixed values at the inlet boundary were determined by assuming a freestream turbulence intensity of 0.1%, resulting in being 1.11×10^{-4} m^2/s^2 and 0.45 s^{-1}, for the turbulent kinetic energy and the specific turbulent dissipation ratio, respectively.

2.4 CFD Solver

The simulations were conducted using the open-source CFD toolkit OpenFOAM. Following the FV approach, each computational cell was considered as a control volume, where discrete versions of the conservation laws are imposed [13]. In this study, we use the *rhoPimpleFoam* solver, which employs the PIMPLE scheme to solve the transient, turbulent compressible flow governing equations. The numerical method combines the PISO and SIMPLE algorithms for computing the pressure field. For the time discretization, the Crank-Nicolson Scheme with an off-centering coefficient of 0.33 was used. The second-order linear upwind scheme was used for pressure, momentum and turbulence variables. To achieve a good convergence rate, the convergence criterion and the under-relaxation factors were properly tuned. Moreover, for all other flow variables, the smoothSolver with the symmetric Gauss-Seidel smoother was used. The adaptive time-step size was determined by setting the maximum Courant number of 0.5 for the transient calculation.

3 Results

The predicted mean flow around the blade is illustrated in Fig. 4, where the contour maps of mean pressure and velocity modulus are reported for four different cross-sections, corresponding to 40%, 60%, 80%, and 90% of the blade length. The corresponding contour maps of density and flow Mach number are depicted in Fig. 5. As was expected, the density variations are significant, as the local flow conditions approach the compressibile regime. This effect is more pronounced at high distance form the rotation axis, due to the high relative wind velocity. Moreover, the highest deviation from the ambient air density, which was chosen as $\rho_\infty = 1.22\ kg/m^3$, occurs on the suction side of the blade. This is

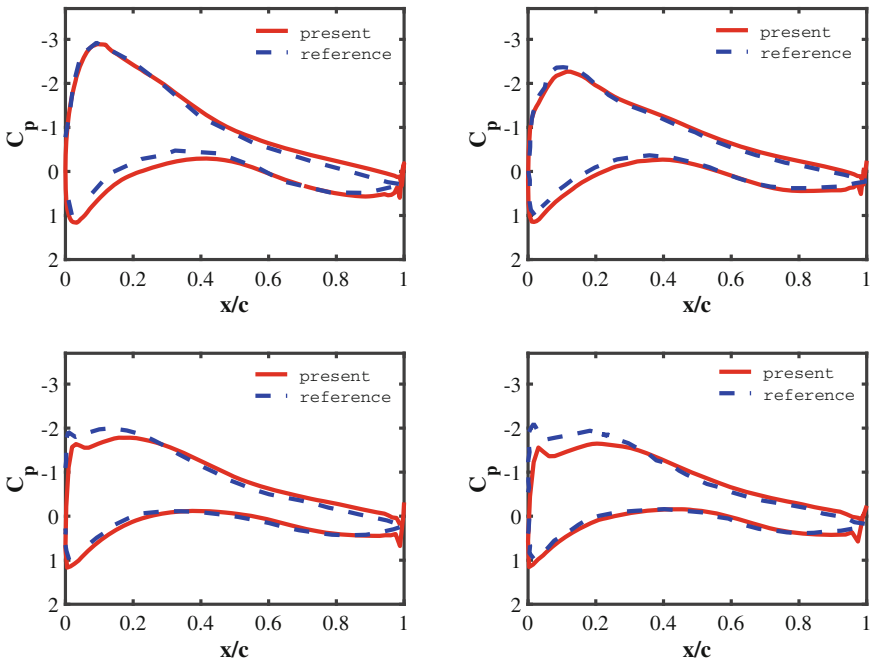

Fig. 7. Sectional pressure coefficient distribution for four different blade cross-sections at 40% (top left), 60% (top right), 80% (bottom left), and 90% (bottom right) span, compared to reference data.



Fig. 8. Limiting streamlines on pressure (top) and suction (bottom) sides of the blade.

clearly demonstrated by looking at the Mach number contours. Apparently, the flow region with large Mach number increases, along with the maximum value of this parameter, with the cross-section station moving towards the blade tip. The location of the maximum Mach number, for each blade section, is close to the leading edge, where the air speed increases due to the high expansion. Furthermore, the relative surface pressure $\Delta p = p - p_\infty$ on the blade is drawn in Fig. 6, for both suction and pressure sides.

From a quantitative point of view, the pressure distribution on the blade surface was examined by estimating the sectional pressure coefficient that is defined by:

$$C_p = \frac{\Delta p}{\frac{1}{2}\rho_\infty \left(U_\infty^2 + \Omega^2 \mathrm{r}^2\right)} \tag{1}$$

where r is the distance for the rotation axis. Note that the reference dynamic pressure is corresponding to the relative wind velocity. Figure 7 shows the sectional pressure coefficient distribution at the same cross-sections considered in the previous figures, with the present results being compared against the reference RANS solution [14]. Note that the reference simulation used the standard k-ϵ model for the same RWT model under investigation. The agreement between the two different solutions is pretty good, taking also into account the reduced size of the present FV grid. However, the numerical resolution of the trailing edge region should be suitably increased. In fact, the generation and testing of finer grids were deferred to future work.

The solution is further examined by looking at the limiting streamlines demonstrating the strong three-dimensional character of the flow on the turbine blade. Figure 8 shows the streamlines on both pressure and suction sides of the blade. The fluid moves down the blade towards the tip, and towards the leading edge. After reaching the leading edge region, it is swept off the blade in

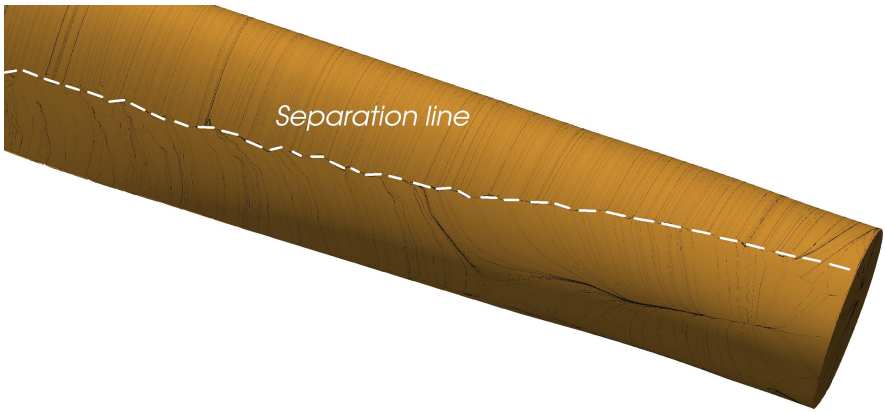

Fig. 9. Separated flow visualization on the suction side, near the blade root (right bottom corner).

the separation shear layer. The separation line on the suction side of the blade is visualized in Fig. 9, where the flow is demonstrated to be highly separated in the blade root region. In fact, this separation line becomes less pronounced moving along the blade towards the tip.

Finally, the WT blade performance is examined by looking at the predicted thrust that is the force experienced by the turbine in the direction parallel to airflow. After the initial transient, the thrust reaches an approximate value of 2.5 MN, which slightly differs from the reference value of 2.2 MN [14]. Note that the present unsteady simulation used a fully three-dimensional computational domain, whereas the reference steady solution was obtained for one third of this domain, while employing peridodic boundary conditions in the azimuthal direction.

4 Conclusions and Perspectives

The present study has to be intended as the proof-of-concept, namely, the preliminary development of a CFD prediction tool using the OpenFOAM software for studying the compressible aerodynamics of a modern wind turbine. The CFD analysis of a 15 MW wind turbine blade model was performed under normal operating conditions. The observed characteristics were in acceptable agreement, both qualitatively and quantitatively, with the data available from a steady flow simulation of the same turbine model. This work paves the way for directly investigating the effects of compressibility on the blade aerodynamics of relevance to modern type large scale wind turbine rotors, using open source software. This research shows that it is possible to successfully simulate the compressible aerodynamics of these systems using the unsteady compressible RANS approach, instead of using compressibility corrections. However, the present CFD model needs further improvement to be effectively used for the aerodynamic design of the whole three-blade rotor.

As to future perspectives, there remains the possibility of developing more sophisticated computational models for this particular wind engineering application, pursuing higher levels of accuracy. For instance, the wavelet-based adaptive multiscale approach for aerodynamic turbulent flows is subject of ongoing research [15,16]. This innovative methodology exploits the wavelet transform to dynamically and automatically adjust the grid resolution to the local flow conditions [17,18]. Wavelet-based adaptive unsteady RANS modelling procedures that have been recently developed [19,20] will be explored in this context, even considering the possibility of supersonic flow on near-future large wind turbines [21]. Finally, the use of higher-fidelity scale-resolving simulation methods, such as wall-modeled hybrid RANS-LES [22], will be subject of future investigation.

References

1. Yan, C., Archer, C.L.: Assessing compressibility effects on the performance of large horizontal-axis wind turbines. Appl. Energy **212**, 33–45 (2018)
2. Sørensen, J.N.; Bertagnolio, F.; Jost, E.; Lutz, T. Aerodynamic effects of compressibility for wind turbines at high tip speeds. J. Phys.: Conf. Ser. **1037**, 022003 (2018)
3. Sørensen, J.N.: Aerodynamic aspects of wind energy conversion. Annu. Rev. Fluid Mech. **43**, 427–448 (2011)
4. Madsen, M.H.A., Zahle, F., Sørensen, N.N., Martins, J.R.R.A.: Multipoint high-fidelity CFD-based aerodynamic shape optimization of a 10 MW wind turbine. Wind Energ. Sci. **4**, 163–192 (2019)
5. Wilcox, D.C.: Turbulence Modeling for CFD, 3rd edn. DCW Industries Inc, La Canada CA (2006)
6. Hossain, M.A., Ziaul, H., Kommalapati, R.R., Khan, S.: Numeric investigation of compressible flow over NREL Phase VI airfoil. Int. J. Eng. Res. Technol. **2**, 2 (2013)
7. Gaertner, E.; Rinker, J.; Sethuraman, L. et al. Definition of the IEA 15-Megawatt Offshore Reference Wind Turbine, NREL/TP-75698, International Energy Laboratory (2020)
8. IEA Wind Task 37 Model data for the 15 MW offshore reference wind turbine. https://github.com/IEAWindTask37/IEA-15-240-RWT Accessed 03 Jan 2023
9. Song, X., Perot, J.B.: CFD Simulation of the NREL Phase VI Rotor. Wind Eng. **39**, 299–310 (2015)
10. De Stefano, G., Natale, N., Reina, G.P., Piccolo, A.: Computational evaluation of aerodynamic loading on retractable landing-gears. Aerospace **7**, 68 (2020)
11. Natale, N., Salomone, T., De Stefano, G., Piccolo, A.: Computational evaluation of control surfaces aerodynamics for a mid-range commercial aircraft. Aerospace **7**, 139 (2020)
12. Menter, F.R.: Two-equation eddy-viscosity turbulence models for engineering applications. AIAA J. **32**, 1598–1605 (1994)
13. Denaro, F.M., De Stefano, G.: A new development of the dynamic procedure in large-eddy simulation based on a finite volume integral approach. Theor. Comput. Fluid Dyn. **25**, 315–355 (2011)
14. Cao, J., et al.: Study of air compressibility effects on the aerodynamic performance of the IEA-15 MW offshore wind turbine. Energy Conv. Manag. **282**, 116883 (2023)
15. De Stefano, G., Dymkoski, E., Vasilyev, O.V.: Localized dynamic kinetic-energy model for compressible wavelet-based adaptive large-eddy simulation. Phys. Rev. Fluids **7**, 054604 (2022)
16. De Stefano, G.: Wavelet-based adaptive large-eddy simulation of supersonic channel flow with different thermal boundary conditions. Phys. Fluids **35**, 035138 (2023)
17. De Stefano, G., Brown-Dymkoski, E., Vasilyev, O.V.: Wavelet-based adaptive large-eddy simulation of supersonic channel flow. J. Fluid Mech. **901**, A13 (2020)
18. Ge, X., De Stefano, G., Hussaini, M.Y., Vasilyev, O.V.: Wavelet-based adaptive eddy-resolving methods for modeling and simulation of complex wall-bounded compressible turbulent flows. Fluids **6**, 331 (2021)
19. Ge, X., Vasilyev, O.V., De Stefano, G., Hussaini, M.Y.: Wavelet-based adaptive unsteady Reynolds-averaged Navier-Stokes computations of wall-bounded internal and external compressible turbulent flows. In: Proceedings of the 2018 AIAA Aerospace Sciences Meeting, Kissimmee, Florida, January (2018)

20. Ge, X., Vasilyev, O.V., De Stefano, G., Hussaini, M.Y.: Wavelet-based adaptive unsteady Reynolds-averaged Navier-Stokes simulations of wall-bounded compressible turbulent flows. AIAA J. **58**, 1529–1549 (2020)
21. De Tavernier, D.; von Terzi, D. The emergence of supersonic flow on wind turbines. J. Phys.: Conf. Ser. **2265**, 042068 (2022)
22. Salomone, T., Piomelli, U., De Stefano, G.: Wall-modeled and hybrid large-eddy simulations of the flow over roughness strips. Fluids **8**, 10 (2023)